The Astrophysical Journal, 805:117 (6pp), 2015 June 1 doi:10.1088/0004-637X/805/2/117

OGLE-2013-BLG-0578 L: A MICROLENSING BINARY COMPOSED OF A BROWN DWARF AND AN M DWARF

H. Park[1], A. Udalski[2,5], C. Han[1,6]
and
R. Poleski[2,3], J. Skowron[2], S. Kozłowski[2], Ł. Wyrzykowski[2,4], M. K. Szymański[2], P. Pietrukowicz[2], G. Pietrzyński[2], I. Soszyński[2], K. Ulaczyk[2]
(The OGLE Collaboration)
[1] Department of Physics, Institute for Astrophysics, Chungbuk National University, Cheongju 371-763, Korea
[2] Warsaw University Observatory, Al. Ujazdowskie 4, 00-478 Warszawa, Poland
[3] Department of Astronomy, Ohio State University, 140 West 18th Avenue, Columbus, OH 43210, USA
[4] Institute of Astronomy, University of Cambridge, Madingley Road, Cambridge CB3 0HA, UK
Received 2015 March 11; accepted 2015 March 25; published 2015 May 27

ABSTRACT

Determining the physical parameters of binary microlenses is hampered by the lack of information about the angular Einstein radius due to the difficulty involved in resolving caustic crossings. In this paper, we present an analysis of the binary microlensing event OGLE-2013-BLG-0578, for which the caustic exit was precisely predicted in advance from real-time analysis, enabling us to densely resolve the caustic crossing and to measure the Einstein radius. From the mass measurement of the lens system based on the Einstein radius, combined with additional information about the lens parallax, we determine that the lens is a binary composed of a late-type M dwarf primary and a substellar brown dwarf companion. This event demonstrates the capability of current real-time microlensing modeling and the usefulness of microlensing for detecting and characterizing faint or dark objects in the Galaxy.

Key words: binaries: general – brown dwarfs – gravitational lensing: micro

1. INTRODUCTION

Low-mass stars comprise a significant fraction of the stars in the Solar neighborhood and the Galaxy as a whole. The Galaxy may be teeming with even smaller mass brown dwarfs. Therefore, studying the abundances and properties of low-mass stars and brown dwarfs is of fundamental importance. There have been surveys that searched for very low-mass (VLM) objects (Reid et al. 2008; Aberasturi et al. 2014), but these surveys were limited to the immediate solar neighborhood. As a result, our sample of VLM objects is small despite their intrinsic abundance, and thus our understanding of VLM objects is poor.

Microlensing surveys detect objects by their gravitational fields rather than their radiation, and thus microlensing can provide a powerful probe of VLM objects. However, the weakness of microlensing is that it is difficult to determine the lens mass for general microlensing events. This difficulty arises due to the fact that the timescale of an event, which is the only observable related to the physical lens parameters, results from the combination of the lens mass and distance, and the relative lens-source transverse speed. As a result, it is difficult to identify and characterize VLM objects although a significant fraction of lensing events are believed to be produced by these objects.

However, it is possible to uniquely determine the physical lens parameters, and thus to identify VLM objects for a subset of lensing events produced by lenses composed of two masses. For unique determinations of physical lens parameters, it is necessary to simultaneously measure the angular Einstein radius $\theta_{\rm E}$ and the microlens parallax $\pi_{\rm E}$ related to the lens mass M and distance to the lens D_L by

$$M_{\rm tot} = \frac{\theta_{\rm E}}{\kappa \pi_{\rm E}}; \qquad D_L = \frac{\rm AU}{\pi_{\rm E}\theta_{\rm E} + \pi_S}, \tag{1}$$

respectively (Gould 2000). Here, $\kappa = 4G/(c^2\ {\rm AU})$, $\pi_S = {\rm AU}/D_S$ is the parallax of the source star, and D_S is the distance to the source. The angular Einstein radius is estimated by analyzing deviations in the lensing light curves caused by the finite size of the lensed source stars (Gould 1994; Nemiroff & Wickramasinghe 1994; Witt & Mao 1994). For single-lens events, finite-source effects can be detected only for a very small fraction of extremely high-magnification events where the lens-source separation at the peak magnification is comparable to or smaller than the source size. On the other hand, the light curves of binary-lens events usually result from caustic crossings during which finite-source effects become important, and thus the chance to detect finite-source effects and measure the Einstein radius is high. Furthermore, binary-lens events tend to have longer timescales than single-lens events, which also contributes to the higher chance of measuring the lens parallax. In fact, most known VLM lensing objects have been identified through the channel of binary-lens events (Hwang et al. 2010; Shin et al. 2012; Choi et al. 2013; Han et al. 2013; Park et al. 2013; Jung et al. 2015), compared to the just one case of an isolated VLM with a measured microlensing mass (Gould et al. 2009).

Despite the usefulness of binary-lens events, the chance to identify VLM objects has been low. One important reason for the low chance is that caustic crossings last for very short

[5] The OGLE Collaboration.
[6] Corresponding author.

periods of time. The duration of a caustic crossing is

$$t_{\rm cc} = \frac{2\rho}{\sin\phi} t_{\rm E}, \quad (2)$$

where $t_{\rm E}$ is the Einstein timescale of the event, ϕ is the entrance angle of the source star with respect to the caustic line, and $\rho = \theta_*/\theta_{\rm E}$ is the angular source radius θ_* normalized to the angular Einstein radius $\theta_{\rm E}$. Considering that the Einstein timescale is $\sim(\mathcal{O})$ 10 days and the Einstein radius is $\sim(\mathcal{O})$ milliarcsec for typical Galactic microlensing events, the duration of a caustic crossing is $\sim(\mathcal{O})$ hr for Galactic bulge source stars with angular stellar radii of $\sim(\mathcal{O})$ 1–10 mas. Therefore, it is difficult to densely resolve caustic crossings from surveys that are being carried out with observational cadences that are lower than one per hour.

Another reason for the low chance of resolving caustic crossings is the difficulty involved in predicting their occurrence. Caustics produced by a binary lens form single or multiple sets of closed curves, and thus caustic crossings always come in pairs. Although it is difficult to predict the first crossing (caustic entrance) based on the fraction of the light curve before the caustic entrance, the second crossing (caustic exit) is guaranteed after the caustic entrance. To resolve the short-lasting caustic exit, it is required to precisely predict the time of the caustic crossing so that observation can be focused to resolve caustic crossings. This requires vigilant modeling of a lensing event conducted over the course of the event followed by intensive follow-up observation.

In this paper, we report the discovery of a VLM binary which was detected from the caustic-crossing binary-lens microlensing event OGLE-2013-BLG-0578. The caustic exit of the event was precisely predicted by real-time modeling, enabling dense resolution and complete coverage of the caustic crossing. Combined with the Einstein radius measured from the caustic-crossing part of the light curve and the lens parallax measured from the long-term deviation induced by Earth's parallactic motion, we uniquely measure the lens mass and determine that the lens is a VLM binary composed of a low-mass star and a brown dwarf.

2. OBSERVATION

The microlensing event OGLE-2012-BLG-0578 occurred on a star located in the direction of the Galactic Bulge. The equatorial coordinates of the lensed star are $(\alpha, \delta)_{\rm J2000} = (17^{\rm h}59^{\rm m}59\overset{\rm s}{.}85, -29°44'06\overset{''}{.}9)$, which correspond to the Galactic coordinates $(l, b) = (0\overset{\circ}{.}90, -3\overset{\circ}{.}10)$. The event was first noticed on 2013 April 22 from survey observations conducted by the Optical Gravitational Lensing Experiment (OGLE: Udalski 2003) using the 1.3 m Warsaw telescope at the Las Campanas Observatory in Chile. Images were taken primarily in the I-band filter and some V-band images were also taken to constrain the lensed star (source).

In Figure 1, we present the light curve of the event. The light curve shows two distinctive spikes which are characteristic features of a caustic-crossing binary-lens event. The caustic crossings occurred at HJD′ = HJD−2450000 ∼ 6426.0 and 6461.8. Although the event was first noticed before the caustic crossings, the caustic entrance was missed. As the event progressed, it became clear that the event was produced by a binary lens from the characteristic "U"-shaped trough between the caustic crossings.

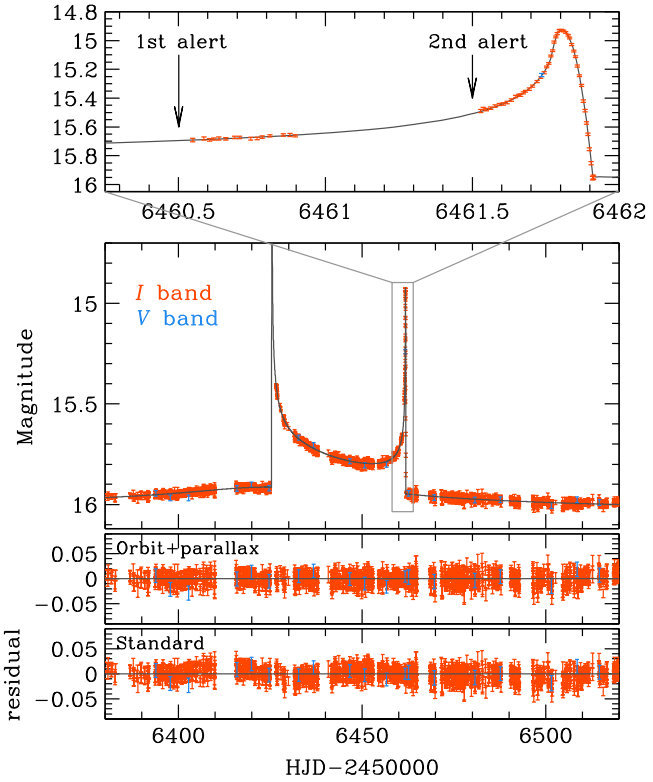

Figure 1. Light curve of OGLE-2013-BLG-0578. Also plotted is the best-fit model ("orbit+parallax" model with $u_0 > 0$). The two bottom panels show the residuals from the modeling with and without considering lens orbital and parallax effects. The upper panel shows the enlargement of the caustic exit region and the times of caustic-crossing alerts.

Although the first caustic crossing was missed, the second crossing was densely resolved. Resolving the crossing became possible with the prediction of the caustic crossing from vigilant modeling of the light curve followed by intensive follow-up observation. It is known that reliable prediction of the second caustic crossing is difficult based on the light curve before the minimum between the two caustic crossings (Jaroszyński and Mao 2001). With the emergence of the correct model after passing the caustic trough, we focused on predicting the exact caustic-crossing time. The first alert of the caustic exit was issued on 2013 June 17, 1.3 days before the actual caustic exit. On the next day, the second alert was issued to predict a more refined time for the caustic exit. In response to the alert, the OGLE experiment, which is usually operated in survey mode, began "following-up" mode observations by increasing the observation cadence. Figure 2 shows the change in the observational cadence during the caustic crossing. The cadence remained close to the normal cadence for this field (about one per 20 minutes) until HJD′ ∼ 6461.75, when it increased to about 1 per 10 minutes. Then, it further increased to 1 per 7 minutes at HJD′ ∼ 6461.88, about halfway down the caustic exit. Thanks to the intensive follow-up observations, the caustic exit was completely and densely covered.

In order to securely measure the baseline magnitude and detect possible higher-order effects, observations continued after the caustic exit to the end of the Bulge season. From these observations, we obtained 2284 and 27 images taken in the I and V bands, respectively. Photometry of the event was performed using a customized pipeline (Udalski 2003) based on the Difference Imaging Analysis method (Alard &

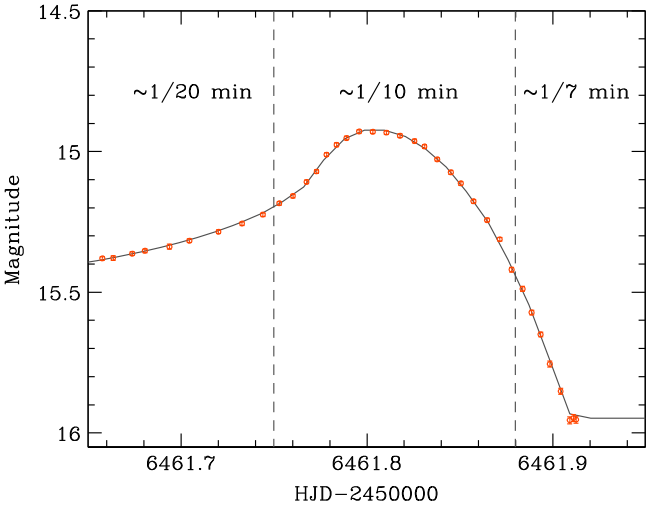

Figure 2. Change of the observational cadence during the caustic exit.

Lupton 1998; Woźniak 2000). We note that the *I*-band data are used for light curve analysis, while the *V*-band data are used to investigate the source type.

It is known that the photometric errors estimated by an automatic pipeline are often underestimated, and thus the errors should be readjusted. We readjust the error bars by

$$e' = k\left(e^2 + e_{\rm min}^2\right)^{1/2}. \quad (3)$$

Here, $e_{\rm min}$ is a term used to make the cumulative distribution function of χ^2 as a function of lensing magnification becomes linear. This process is needed to ensure that the dispersion of data points is consistent with the error bars of the source brightness. The other term k is a scaling factor used to make χ^2 per degree of freedom becomes unity. The adopted coefficients are $k = 2.05$ and $e_{\rm min} = 0.001$ mag.

3. ANALYSIS

We analyze the event by searching for the lensing parameters (lensing solution) that best describe the observed light curve. The basic description of a binary-lens event requires seven standard lensing parameters. Three of these parameters describe the source-lens approach, including the time of the closest approach of the source to a reference position of the lens, t_0, the lens-source separation at t_0 in units of the Einstein radius, u_0, and the time required for the source to cross the Einstein radius, $t_{\rm E}$ (Einstein timescale). In our analysis, we set the center of the mass of the binary lens as a reference position in the lens plane. Another two parameters describe the binary lens, including the projected binary separation in units of the Einstein radius, s (normalized separation), and the mass ratio between the lens components, q. Due to the asymmetry of the gravitational field around the binary lens, it is necessary to define the angle between the source trajectory and the binary axis, α (source trajectory angle). The last parameter is the normalized source radius ρ, which is needed to describe the caustic-crossing parts of the light curve which are affected by finite-source effects.

It is often necessary to consider higher-order effects in order to precisely describe lensing light curves, and this requires that we include additional lensing parameters. For long timescale events, such effects are caused by the positional change of an observer induced by the orbital motion of the Earth around the Sun ("parallax effect": Gould 1992) and/or the change of the binary separation and orientation caused by the orbital motion of the lens ("lens orbital effect": Dominik 1998; Albrow et al. 2000). The analyzed event lasted throughout the whole Bulge season, and thus these effects can be important. The parallax effect is described by two parameters, $\pi_{{\rm E},N}$ and $\pi_{{\rm E},E}$, which are the two components of the lens parallax vector $\boldsymbol{\pi}_{\rm E}$ projected onto the sky along the north and east equatorial coordinates, respectively. The direction of the lens parallax vector corresponds to the relative lens-source proper motion and its magnitude corresponds to the relative lens-source parallax $\pi_{\rm rel} = {\rm AU}(D_L^{-1} - D_S^{-1})$ scaled to the Einstein radius of the lens, i.e.,

$$\pi_{\rm E} = \frac{\pi_{\rm rel}}{\theta_{\rm E}}. \quad (4)$$

To first-order approximation, the lens orbital effect is described by two parameters, ds/dt and $d\alpha/dt$, which are the change rates of the normalized binary separation and the source trajectory angle, respectively.

To model the caustic-crossing parts of the light curve, it is necessary to compute the magnifications affected by finite-source effects. To compute finite-source magnifications, we use the numerical method of the inverse ray-shooting technique (Kayser et al. 1986; Schneider & Weiss 1986) in the immediate neighboring region around caustics and the semi-analytic hexadecapole approximation (Gould 2008; Pejcha and Heyrovský 2009) in the outer region surrounding caustics. We consider the effects of the surface brightness variation of the source star. The surface brightness is modeled as

$$S_\lambda \propto 1 - \Gamma_\lambda\left(1 - \frac{3}{2}\cos\psi\right), \quad (5)$$

where Γ_λ is the linear limb-darkening coefficient, λ is the passband, and ψ is the angle between the line of sight toward the source star and the normal to the source surface. We adopt the limb-darkening coefficients $(\Gamma_V, \Gamma_I) = (0.62, 0.45)$ from Claret (2000) based on source type. The source type is determined based on its de-reddened color and brightness. See Section 4 for details about how the source type is determined.

The search for the best-fit solution of the lensing parameters is carried out based on the combination of the grid-search and downhill approaches. We set (s, q, α) as the grid parameters because lensing magnifications can vary dramatically with small changes of these parameters. On the other hand, magnifications vary smoothly with changes in the remaining parameters, and thus we search for these parameters using a downhill approach. We use the Markov Chain Monte Carlo (MCMC) method for the downhill approach. Searching for solutions throughout the grid-parameter spaces is important because it enables us to check the possible existence of degenerate solutions where different combinations of the lensing parameters result in similar light curves.

In the initial search for solutions, we conduct modeling of the light curve based on the seven basic binary-lensing parameters ("standard model"). From this, it is found that the event was produced by a binary with a projected separation very close to the Einstein radius, i.e., $s \sim 1.0$. Caustics for such a resonant binary form a single large closed curve with six

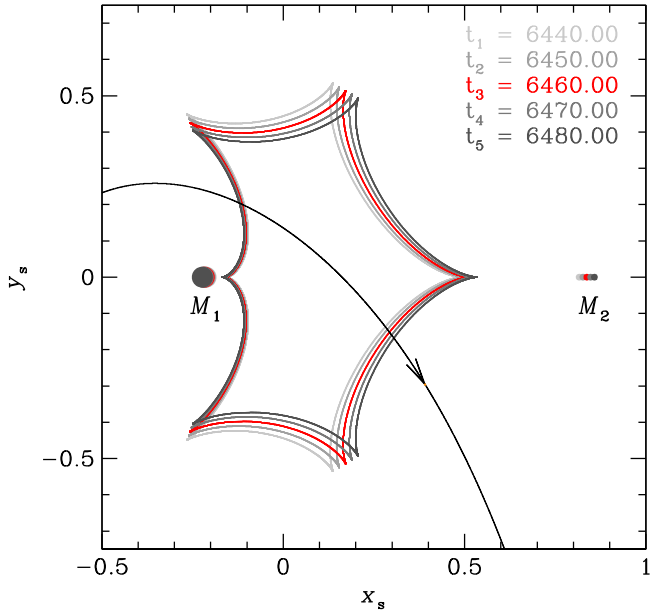

Figure 3. Source trajectory (the curve with an arrow) with respect to the caustic (the closed curve with six cusps). The two small dots marked by M_1 and M_2 represent the positions of the binary lens components. All lengths are scaled by the angular Einstein radius corresponding to the total mass of the binary lens. Due to the change of the relative positions of the binary lens components caused by the orbital motion, the caustic varies in time. We present four caustics and lens positions corresponding to the times marked in upper right corner of the panel. The source trajectory is curved due to the combination of the lens orbital and parallax effects.

cusps. The two spikes of the light curve were produced by the source trajectory passing diagonally through the caustic. See Figure 3 where we present the source trajectory with respect to the caustic.[7] The estimated mass ratio between the binary components is $q \sim 0.2$–0.3.

Although the standard model provides a fit that matches the overall pattern of the observed light curve, it is found that there exists some residual in the region around HJD′ $\sim$ 6410. See the bottom panel of Figure 1. We therefore check whether higher-order effects improve the fit. We find that separate consideration of the parallax effect ("parallax model") and the lens orbital effect ("orbital model") improves the fit by $\Delta\chi^2 = 579$ and 344, respectively. When both effects are simultaneously considered ("orbit+parallax model"), the fit improves by $\Delta\chi^2 = 616$, implying that both effects are important. In Figure 4, we present the contours of $\Delta\chi^2$ in the space of the higher-order lensing parameters. The contours marked in different colors represent the regions with $\Delta\chi^2 < 1$ (red), 4 (yellow), 9 (green), 16 (sky blue), 25 (blue), and 36 (purple). This shows that the higher-order effects are clearly detected. Considering the time gap between the caustic crossings, which is approximately a month, and the long duration of the event, which lasted throughout the whole Bulge season, the importance of the higher-order effects is somewhat expected.

It is known that lensing events with higher-order effects are subject to degeneracy caused by the mirror symmetry of the source trajectory with respect to the binary axis (Skowron et al. 2011). This so-called "ecliptic degeneracy" is important for Galactic Bulge events which occur near the ecliptic plane. The pair of solutions resulting from this degeneracy have almost identical parameters except $(u_0, \alpha, \pi_{E,N}, d\alpha/dt) \rightarrow -(u_0, \alpha, \pi_{E,N}, d\alpha/dt)$. It is found that $u_0 > 0$ is marginally preferred over the $u_0 < 0$ solution by $\Delta\chi^2 = 25.0$, which corresponds formally to a $\sim 5\sigma$ level difference. However, this level of $\Delta\chi^2$ can often occur due to systematics in the data, and thus one cannot completely rule out the $u_0 < 0$ solution. In Table 1, we present the best-fit parameters of both $u_0 > 0$ and $u_0 < 0$ solutions. We note that the uncertainties of the lensing parameters are estimated based on the distributions of the parameters obtained from the MCMC chain of the solution. We also present the best-fit model light curve ($u_0 > 0$ solution) and the corresponding source trajectory with respect to the lens and caustic in Figures 1 and 3, respectively.

4. PHYSICAL PARAMETERS

By detecting both finite-source and parallax effects, one can measure the angular Einstein radius and the lens parallax, which are the two quantities needed to determine the mass and distance to the lens. The lens parallax is derived by $\pi_E = (\pi_{E,N}^2 + \pi_{E,E}^2)^{1/2}$ from the parallax parameters determined from light curve modeling.

In order to estimate the angular Einstein radius, it is necessary to convert the measured normalized source radius ρ into θ_E using the angular radius of the source star, i.e., $\theta_E = \theta_*/\rho$. The angular source radius is estimated based on the de-reddened color $(V-I)_0$ and brightness I_0 of the source star, which are calibrated using the centroid of the Bulge giant clump on the color-magnitude diagram as a reference (Yoo et al. 2004). By adopting the color and brightness of the clump centroid $(V-I, I)_{0,c} = (1.06, 14.45)$ (Bensby et al. 2011; Nataf et al. 2013), we estimate that $(V-I, I)_0 = (0.72, 17.68)$ for the source star, implying that the source star is a G-type subgiant. Figure 5 shows the locations of the source and the centroid of the giant clump in the color-magnitude diagram of stars around the source star. We then translate $V-I$ into $V-K$ using the color–color relation of Bessell & Brett (1988) and obtain the angular source radius using the relation between $V-K$ and θ_* from Kervella et al. (2004). The determined angular source radius is $\theta_* = 0.93 \pm 0.06\ \mu$as. Then, the Einstein radius is estimated as $\theta_E = 0.97 \pm 0.07$ mas for the best-fit solution ($u_0 > 0$ model). The $u_0 < 0$ model results in a similar Einstein radius due to the similarity in the measured values of ρ. Combined with the measured Einstein timescale t_E, the relative lens-source proper motion is estimated as $\mu = \theta_E/t_E = 4.90 \pm 0.35$ mas yr^{-1}. We note that the reference time for μmeasurement is t_0.

With the measured lens parallax and Einstein radius, we determine the mass and the distance to the lens using Equation (1). In Table 2, we list the physical parameters of the lens system corresponding to the $u_0 > 0$ and $u_0 < 0$ solutions. We note that the estimated parameters from the two solutions are similar. According to the estimated mass, the lens system is composed of a substellar brown dwarf companion and a late-type M-dwarf primary. The distance to the lens is $D_L < 1.2$ kpc, and thus the lens is located in the Galactic disk. The projected separation between the lens components is $r_\perp = sD_L\theta_E$ is slightly greater than 1 AU.

In order to check the validity of the obtained lensing solution, we compute the projected kinetic to potential energy

[7] We note that the source trajectory is curved due to the combination of the lens orbital and parallax effects. We also note that the caustic varies in time due to the positional change of the binary lens components caused by the orbital motion.

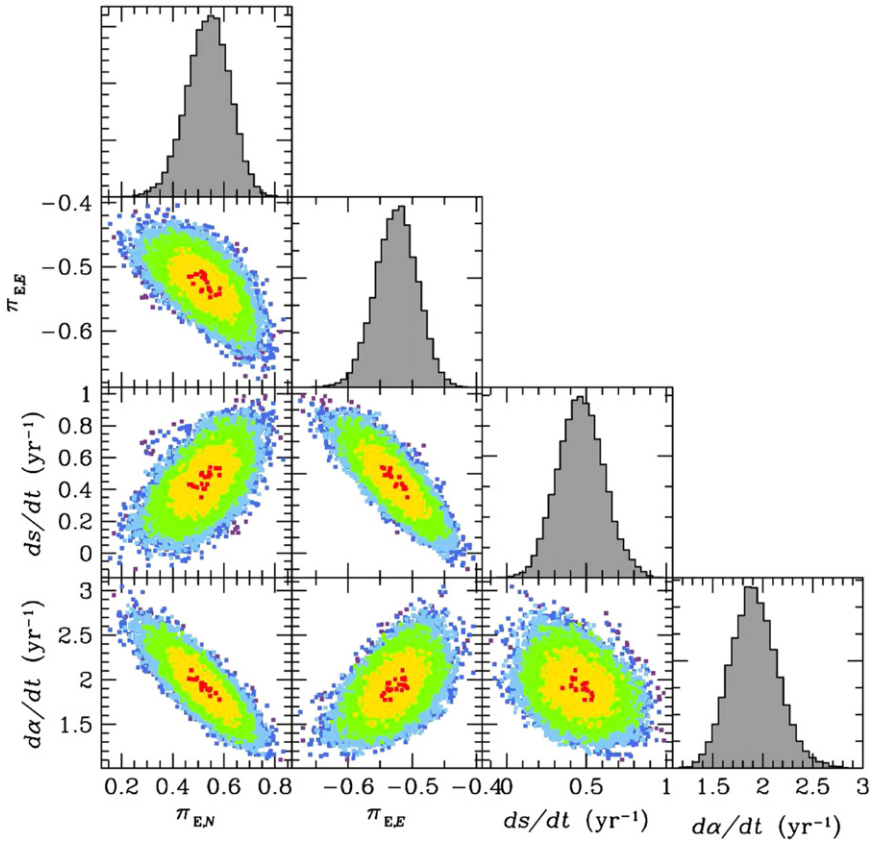

Figure 4. Contours of $\Delta\chi^2$ in the space of the parallax and lens orbital parameters for the best-fit model ($u_0 > 0$ model). The contours marked in different colors represent the regions with $\Delta\chi^2 < 1$ (red), 4 (yellow), 9 (green), 16 (sky blue), 25 (blue), and 36 (purple).

Table 1
Lensing Parameters

Parameter	$u_0 > 0$	$u_0 < 0$
χ^2/dof	2303.1/2300	2328.1/2300
t_0 (HJD)	2456440.13 ± 0.11	2456439.99 ± 0.08
u_0	0.109 ± 0.004	−0.120 ± 0.003
t_E (days)	72.11 ± 0.84	70.79 ± 0.10
s	1.027 ± 0.004	1.035 ± 0.002
q	0.260 ± 0.004	0.241 ± 0.003
α (rad)	0.676 ± 0.007	−0.647 ± 0.007
ρ (10^{-3})	0.96 ± 0.01	0.97 ± 0.01
$\pi_{E,N}$	0.54 ± 0.08	−0.51 ± 0.05
$\pi_{E,N}$	−0.53 ± 0.03	−0.72 ± 0.02
ds/dt (yr^{-1})	0.48 ± 0.14	0.40 ± 0.03
$d\alpha/dt$ (rad yr^{-1})	1.89 ± 0.24	−1.75 ± 0.13
$(V-I, I)_S$	(1.5, 18.9)	...
$(V-I, I)_b$	(1.0, 16.1)	...

Note. $(V-I, I)_S$ and $(V-I, I)_b$ represent the $V-I$ colors and I-band magnitudes of the source and blend, respectively.

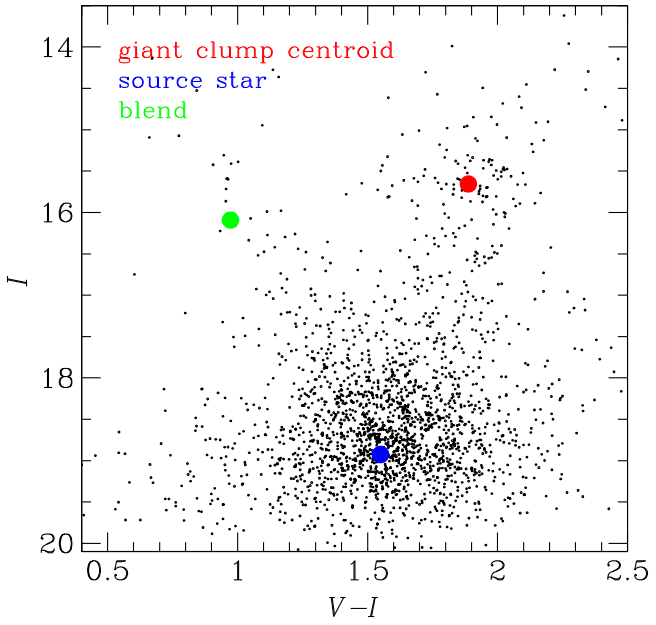

Figure 5. Location of the lensed star with respect to the centroid of giant clump in the color–magnitude diagram of neighboring stars. Also marked is the location of the blend.

ratio $(\mathrm{KE/PE})_\perp$ by

$$\left(\frac{\mathrm{KE}}{\mathrm{PE}}\right)_\perp = \frac{(r_\perp/\mathrm{AU})^3}{8\pi^2(M/M_\odot)}\left[\left(\frac{1}{s}\frac{ds/dt}{\mathrm{yr}^{-1}}\right)^2 + \left(\frac{d\alpha/dt}{\mathrm{yr}^{-1}}\right)^2\right] \quad (6)$$

(Dong et al. 2009). The measured values are $(\mathrm{KE/PE})_\perp = 0.48$ and 0.32 for the $u_0 > 0$ and $u_0 < 0$ solutions, respectively. Since the values are less than unity, they meet the condition of a bound system. Even if $(\mathrm{KE/PE})_\perp < 1$, a high value, e.g., ~0.9, would require a highly eccentric orbit which is seen nearly face on and just happens to be observed at pericenter. The measured values are

Table 2
Physical Parameters

Parameter	$u_0 > 0$	$u_0 < 0$
Einstein radius (mas)	0.97 ± 0.07	0.96 ± 0.07
Geocentric proper motion (mas yr^{-1})	4.90 ± 0.35	4.96 ± 0.35
Heliocentric proper motion vector (mas yr^{-1})	$(0.72 \pm 0.05, 3.70 \pm 0.26)$	$(0.77 \pm 0.05, -2.63 \pm 0.18)$
Total mass ($M_\odot$)	0.156 ± 0.017	0.133 ± 0.011
Mass of primary ($M_\odot$)	0.124 ± 0.014	0.107 ± 0.009
Mass of companion ($M_\odot$)	0.032 ± 0.004	0.026 ± 0.002
Distance (kpc)	1.16 ± 0.11	1.02 ± 0.08
Projected separation (AU)	1.16 ± 0.11	1.02 ± 0.08
$(\mathrm{KE/PE})_\perp$	0.48 ± 0.20	0.32 ± 0.07

Note. The two values of the heliocentric proper motion represent the north and east components.

close to the expected values for roughly circular orbits in random orientations.

It is found that the blend of the event is a disk star with a color and magnitude $(V - I) = (0.97, 16.1)$. See its location on the color-magnitude diagram in Figure 5. Considering that the lens is in the disk, it might be that the blend is the lens itself. If so, then the intrinsic color of the lens primary would be $(V - I)_0 \sim 4.0$. Considering $E(V - I) \sim 0.5$ for a disk star, the apparent color and magnitude of the lens are $(V - I, I) \sim (4.5, 23)$. These values are inconsistent with the measured values of the blend, and thus the blend is unlikely to be the lens. Then, the blend might be a star unrelated to the lens or the blend is part of a hierarchical triple composed of itself and the microlensing binary. The former possibility can be checked by comparing the astrometric positions of the blend at the baseline with that of the magnified source.

5. CONCLUSION

We presented an analysis of the caustic-crossing binary-lens microlensing event OGLE-2013-BLG-0578 which led to the discovery of a binary system composed of a substellar brown dwarf companion and a late-type M-dwarf primary. Identification of the lens became possible due to the prediction of the caustic crossing from vigilant real-time modeling and resolution of the caustic from prompt follow-up observation. The event demonstrates the capability of current real-time modeling and the usefulness of microlensing in detecting and characterizing faint or dark objects in the Galaxy.

Work by C.H. was supported by Creative Research Initiative Program (2009-0081561) of National Research Foundation of Korea. We acknowledge funding from the European Research Council under the European Community's Seventh Framework Programme (FP7/2007-2013)/ERC grant agreement No. 246678 to A.U. for the OGLE project.

REFERENCES

Aberasturi, M., Caballero, J. A., Montesinos, B., et al. 2014, AJ, 148, 36
Alard, C., & Lupton, R. H. 1998, ApJ, 503, 325
Albrow, M. D., Beaulieu, J.-P., Caldwell, J. A. R., et al. 2000, ApJ, 534, 894
Bensby, T., Adén, D., Meléndez, J., et al. 2011, A&A, 533, 134
Bessell, M. S., & Brett, J. M. 1988, PASP, 100, 1134
Choi, J.-Y., Han, C., Udalski, A., et al. 2013, ApJ, 768, 129
Claret, A. 2000, A&A, 363, 1081
Dominik, M. 1998, A&A, 329, 361
Dong, S., Gould, A., Udalski, A., et al. 2009, ApJ, 695, 970
Gould, A. 1992, ApJ, 392, 442
Gould, A. 1994, ApJ, 421, 71
Gould, A. 2000, ApJ, 542, 785
Gould, A. 2008, ApJ, 681, 1593
Gould, A., Udalski, A., Monard, B., et al. 2009, ApJL, 698, L147
Han, C., Jung, Y. K., Udalski, A., et al. 2013, ApJ, 778, 38
Hwang, K.-H., Udalski, A., Han, C., et al. 2010, ApJ, 723, 797
Jaroszyński, M., & Mao, S. 2001, MNRAS, 325, 1546
Jung, Y. K., Udalski, A., Sumi, T., et al. 2015, ApJ, 798, 123
Kayser, R., Refsdal, S., & Stabell, R. 1986, A&A, 166, 36
Kervella, P., Bersier, D., Mourard, D., et al. 2004, A&A, 428, 587
Nataf, D. M., Gould, A., Fouqué, P., et al. 2013, ApJ, 769, 88
Nemiroff, R. J., & Wickramasinghe, W. A. D. T. 1994, ApJ, 424, 21
Park, H., Udalski, A., Han, C., et al. 2013, ApJ, 778, 134
Pejcha, O., & Heyrovský, D. 2009, ApJ, 690, 1772
Reid, I. N., Cruz, K. L., Kirkpatrick, J. D., et al. 2008, AJ, 136, 1290
Schneider, P., & Weiss, A. 1986, A&A, 164, 237
Shin, I.-G., Han, C., Gould, A., et al. 2012, ApJ, 760, 116
Skowron, J., Udalski, A., Gould, A., et al. 2011, ApJ, 738, 87
Udalski, A. 2003, AcA, 53, 291
Witt, H. J., & Mao, S. 1994, ApJ, 430, 505
Woźniak, P. R. 2000, AcA, 50, 421
Yoo, J., DePoy, D. L., Gal-Yam, A., et al. 2004, ApJ, 603, 139